

Crystal structures of two-dimensional magnetic colloids in tilted external magnetic fields

V. A. Froltsov, R. Blaak, C. N. Likos, and H. Löwen

Institut für Theoretische Physik II, Heinrich-Heine-Universität Düsseldorf, Universitätsstraße 1, D-40225 Düsseldorf, Germany

(Received 25 September 2003; published 30 December 2003)

The stability of different crystal lattices of two-dimensional superparamagnetic suspensions that are confined to a planar liquid-gas interface and exposed to a tilted external magnetic field is studied theoretically by lattice sum minimizations. The magnetic field induces magnetic dipoles onto the colloidal particles along its direction, whose strength can be controlled by the amplitude of the external field. The mutual interaction between the colloids is governed by dipole-dipole forces and a short-ranged repulsion having its physical origin at the presence of the colloidal cores. If the direction of the magnetic field is perpendicular to the liquid-gas interface, there is a purely repulsive interaction leading to stable triangular crystals. By tilting the external field, the interaction becomes anisotropic and a mutual attraction appears upon a threshold tilt angle. We have calculated the full phase diagram at zero temperature varying the tilt angle, the colloidal density, and the strength of the magnetic field. Apart from the triangular lattice we find a variety of stable crystal lattices including rectangular, oblique, chainlike oblique, and rhombic structures. We also present the accurate derivation of the Hamiltonian of two polarizable particles of finite arbitrary geometries in external magnetic and electric fields.

DOI: 10.1103/PhysRevE.68.061406

PACS number(s): 82.70.Dd, 64.70.Kb, 61.50.-f

I. INTRODUCTION

Crystallization in colloidal monolayers that are confined to a vapor-liquid interface is a fascinating self-organization process, details of which have been studied recently [1–7]. In particular, superparamagnetic microspheres suspended in a pendant drop in gravity are excellent realizations of strictly two-dimensional classical many-body systems; for recent reviews, see Refs. [8,9]. An additional external magnetic field will induce magnetic dipole moments on the particles, whose direction and strength can easily be tailored via the external field [10]: the dipole moments almost perfectly align along the field direction and the magnitude of the dipole moment is proportional to the field amplitude. In the conventional setup, the magnetic field is perpendicular to the air-water interface, so that the colloidal particles will interact via purely repulsive dipole-dipole forces, additional to the short-ranged repulsion arising from the physical core of the particles. For large magnetic fields, the typical strength of the repulsive interaction is much larger than the thermal energy, enforcing crystallization of the microspheres into a triangular monolayer. It is known that the three-dimensional melting transition [11] can be qualitatively different from that in two spatial dimensions following a two-stage scenario with an intermediate hexatic phase as theoretically predicted by Kosterlitz, Thouless, Nelson, Halperin, and Young (KTNY) [12]. In fact, by using video microscopy and digital image processing, it was shown by Maret and co-workers that two-dimensional superparamagnetic colloidal suspensions indeed follow the KTNY scenario [13–16].

In the present paper, we consider the case of a magnetic field that is *tilted* with respect to the surface of the gas-liquid interface. The reason for doing so is twofold: first, a setup with a tilted external magnetic field can easily be realized in an experiment [17]. Second, more fundamentally, a tilt angle induces an anisotropic interaction and therefore new physics. Furthermore, if the tilt angle φ of magnetic field with its projection on the surface is smaller than 54.7° , the dipole-

dipole interaction exhibits also attractive parts which can give rise to new phenomena. By varying the tilt angle φ , one continuously interpolates between two extreme limits of $\varphi = 0^\circ$ and $\varphi = 90^\circ$, both of which have been already studied: the preceding studies of the melting process invoke a perpendicular field ($\varphi = 90^\circ$), while the parallel field case ($\varphi = 0^\circ$) corresponds to two-dimensional dipoles with a fixed orientation in the plane. The latter model was considered in the context of ferrofluidic monolayers where chain formation has been simulated by Satoh *et al.* [18].

In this paper, we calculate by lattice sum minimization the stable bulk crystalline lattices in the case where the interaction energy between the colloids is much larger than the thermal energy $k_B T$, so that thermal fluctuations can be neglected. As expected, the resulting stable bulk solid structures are strongly anisotropic and different from their counterpart arising from purely repulsive interactions, which is the triangular lattice that has a high degree of isotropy. The anisotropy of the interactions together with the additional attractions generate various two-dimensional crystalline structures such as rectangular, oblique, chainlike oblique, and rhombic lattices. We obtain the whole phase diagram varying the tilt angle, the particle concentration, as well as the magnetic field strength relative to the strength of a short-ranged repulsion that stems from a soft physical colloidal core. Both first- as well as second-order transitions between the different lattice structures are found.

In relation to other previous work, our study is first complementary to those assuming a perpendicular magnetic field ($\varphi = 90^\circ$) but exposing the system to an additional external potential, such as gravity, that leads to the formation of nonhomogeneous conformal crystals [19,20]. Second, in our model the orientation of the dipoles is fixed by the field, which makes our model different from that of orientable dipoles where the dipole orientation is treated as an additional statistical degree of freedom. Such models have been investigated in detail in two spatial dimensions for the sphere centers and the dipolar orientations of the spheres fixed on

the three-dimensional unit sphere [21,22] and two-dimensional unit circle [23]. In the latter case, ring formation of dipolar chains was obtained by computer simulation.

The paper is organized as follows: in Sec. II we define our model; details for the derivation of the Hamiltonian are presented in the Appendix. The lattice sum minimization technique is explained in Sec. III, whereas the resulting phase diagrams are presented and discussed in Sec. IV. Finally, in Sec. V we summarize and conclude.

II. THE MODEL

We consider a system of superparamagnetic colloidal particles interacting with each other via the dipole-dipole pair potential, valid for pointlike magnetic dipoles,

$$u^{\text{dd}}(\mathbf{r}, \mathbf{m}_i, \mathbf{m}_j) = \frac{1}{2} \frac{\mathbf{m}_i \cdot \mathbf{m}_j - 3(\mathbf{m}_i \cdot \mathbf{n})(\mathbf{m}_j \cdot \mathbf{n})}{r^3}, \quad (1)$$

and a truncated-and-shifted Lennard-Jones pair potential:

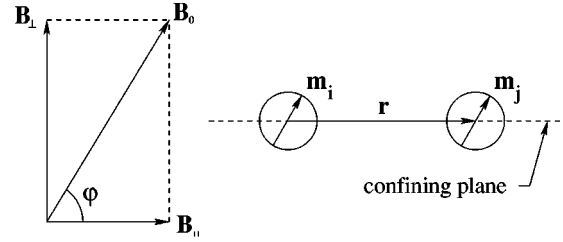
$$u^{\text{LJ}}(r) = \begin{cases} 4\varepsilon \left[\left(\frac{\sigma}{r} \right)^{12} - \left(\frac{\sigma}{r} \right)^6 + \frac{1}{4} \right] & \text{if } r \leq 2^{1/6}\sigma \\ 0 & \text{if } r > 2^{1/6}\sigma, \end{cases} \quad (2)$$

where \mathbf{r} is the interparticle separation vector, $\mathbf{n} = \mathbf{r}/r$ is the unit vector along the line connecting the colloids' centers, \mathbf{m}_i and \mathbf{m}_j are the magnetic moments carried by particles i and j ($i \neq j$), σ is the effective particle diameter, and ε sets the energy scale of the short-ranged soft core repulsion. The factor $1/2$ in Eq. (1) appears due to the paramagnetic nature of colloids, i.e., it stems from the fact that the dipoles on the particles are not permanent but rather induced by the external magnetic field. A detailed derivation of the interaction energy of two polarizable particles in an arbitrarily varying external field is presented in the Appendix. The purely repulsive Lennard-Jones potential, Eq. (2), is used to model the short-ranged repulsion between the physical cores of the particles, whereas dispersion attractions between them are ignored.

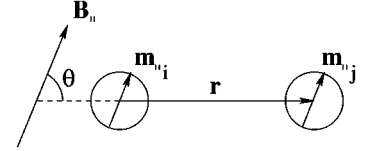
In our problem the colloids are spherical with a finite extent but, for the sake of simplicity, we consider their magnetic dipoles as pointlike. Their motion is confined on the plane formed by the water-air interface. This two-dimensional system consisting of N particles is placed under a spatially homogeneous magnetic field \mathbf{B}_0 , which induces in each particle a magnetic moment \mathbf{m}_i , $i = 1, 2, \dots, N$. Since water has roughly the same magnetic permeability μ as air, the presence of the interface is not relevant from the point of view of the magnetic interactions and thus the derivation in the Appendix (which is carried out in the absence of such physical interfaces) carries over to the problem at hand. In this paper we consider *superparamagnetic* colloids [13] for which the magnetic moment \mathbf{m}_i completely aligns with the external field \mathbf{B}_0 and the following relation holds:

$$\mathbf{m}_i = \chi \mathbf{B}_0,$$

where χ is a magnetic susceptibility of the particles and for the superparamagnetic particles it has a typical value of χ



(a) side view



(b) view from above

FIG. 1. A schematic view of two superparamagnetic colloids confined to a plane and placed in a tilted magnetic field \mathbf{B}_0 . For superparamagnetic particles, the magnetic moments \mathbf{m}_i , \mathbf{m}_j align completely along the external field \mathbf{B}_0 .

$\cong 10^{-11} \text{ A m}^2/\text{T}$ [10]. In this case, in the two-particle Hamiltonian of the system, Eq. (A6), the dipole-field interaction terms $u^{d_1 B_0}$, $u^{d_2 B_0}$ [Eqs. (A3) and (A4)] as well as the field energy u^{B_0} [Eq. (A2)], become irrelevant constants. Thus, for our two-dimensional superparamagnetic particles the dipole-dipole interaction potential (1) takes the form

$$u^{\text{dip}}(\mathbf{r}, \mathbf{B}_0) = u^{\text{dd}}(\mathbf{r}, \chi \mathbf{B}_0, \chi \mathbf{B}_0) = \frac{(\chi B_0)^2}{2} \frac{1}{r^3} (1 - 3 \cos^2 \varphi \cos^2 \theta), \quad (3)$$

where $\cos \theta = \mathbf{r} \cdot \mathbf{B}_{\parallel} / (r B_{\parallel})$, \mathbf{B}_{\parallel} is the in-plane component of the magnetic field, φ is the tilt angle of the magnetic field with respect to the confining plane. We introduce the notation $u^{\text{dip}}(\mathbf{r}, \mathbf{B}_0)$ to discriminate from the general case, Eq. (1). Assuming pair additivity of the interactions, the total Hamiltonian \mathcal{H} of the system takes the form

$$\mathcal{H} = \sum_i \frac{p_i^2}{2m} + \sum_{i < j} [u^{\text{dip}}(\mathbf{r}_i - \mathbf{r}_j) + u^{\text{LJ}}(|\mathbf{r}_i - \mathbf{r}_j|)], \quad (4)$$

where the first term is the total kinetic energy, with the momenta \mathbf{p}_i and the mass m of the particles, and the second is the total potential energy. Since we are going to work at temperature $T=0$ in what follows, the kinetic energy is irrelevant. Figure 1 shows a side view and a view from above for our system, in order to elucidate the considered geometry and the physical setup.

The relative strength of the isotropic truncated and shifted Lennard-Jones interaction and the orientationally dependent dipole-dipole interaction is characterized by the dimensionless coupling constant

$$\lambda = \frac{(\chi B_0)^2}{\sigma^3 \varepsilon}. \quad (5)$$

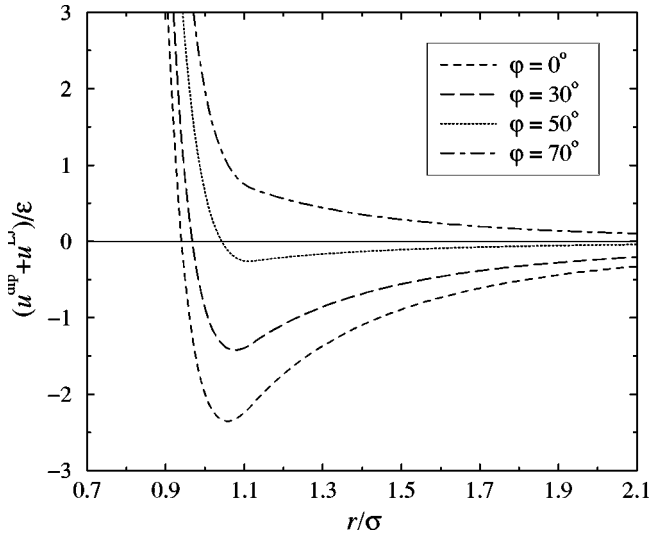


FIG. 2. The total potential of interaction between two superparamagnetic colloidal particles at coupling constant $\lambda=3$, as a function of interparticle separation r . Here the dipoles are fully aligned, $\theta=0$, and the curves correspond to different tilt angles, as indicated in the legend.

Changing of the tilt angle φ of the magnetic field allows for an interplay between the repulsive and attractive contributions of the dipole-dipole interaction. In addition to the steric repulsion, the freedom of varying λ and φ makes the interaction dependent on the relative orientation of the dipoles and offers wide freedom in tailoring the forces between the particles. The dipole-dipole interaction favors fully aligned moments (head-to-tail configurations), as seen in Fig. 2. Due to the presence of the vertical component of the field, net attractions between particles show up for head-to-tail configurations ($\theta=0$) only when the tilt angle φ lies below the threshold value $\arccos(1/\sqrt{3}) \approx 54.7^\circ$.

Our purpose is to find the stable crystal structures formed by the system *at zero temperature*. The area density n of the system is given as $n=N/A$, with the area A occupied by the colloids, and it is understood throughout that the thermodynamic limit is taken. We define the dimensionless area density as $n^*=n\sigma^2$. The problem is thus characterized by three parameters, λ , n^* , and the tilt angle φ of the external field. If the particles arrange themselves in a Bravais lattice, the total energy per particle U_1 is given by the expression

$$U_1 = \frac{1}{2} \sum_{\mathbf{r} \neq 0} [u^{\text{dip}}(\mathbf{r}, \mathbf{B}_0) + u^{\text{LJ}}(r)] + \text{const}, \quad (6)$$

where the sum runs over the set of Bravais lattice vectors and the additive constant includes the irrelevant contributions from the dipole-field interaction and the field energy.

III. CALCULATION OF THE PHASE DIAGRAM

Strictly speaking, the determination of the periodic structure that corresponds to the absolute minimum of the energy is unfeasible: though there are only five Bravais lattices in two dimensions and they can be easily parametrized, one is

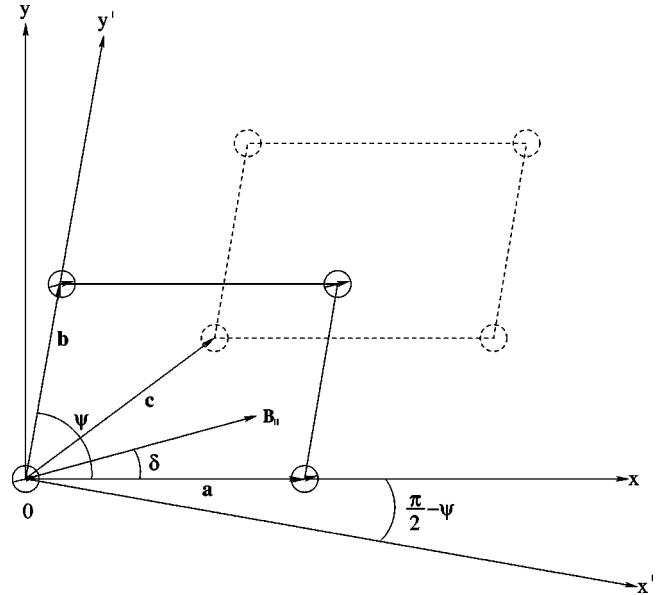


FIG. 3. Geometry of a two-dimensional candidate lattice with one and two particles per unit cell, view from above. Shown are the unit vectors \mathbf{a} and \mathbf{b} of the candidate Bravais lattice with one particle per unit cell, as well as the basis vector \mathbf{c} that characterizes the position of the second particle in the cell, for the case of a lattice with a basis. The small arrows on the particles denote the orientation of the in-plane magnetic dipole moments \mathbf{m}_{\parallel} , which coincides with the direction of \mathbf{B}_{\parallel} . The two different coordinate systems (xy) and $(x'y')$ are introduced for technical reasons in the computation of the lattice sums via the Lekner method; for an explanation see the text.

faced with the additional complication that these can be decorated with bases of an arbitrary number of particles. In order to keep the calculation manageable, we have chosen to restrict ourselves to two classes of periodic structures only: those with one particle per unit cell, which are indeed Bravais lattices, and those with a two-particle basis. The long-range character of the dipole-dipole interaction requires the implementation of special summation techniques and the corresponding formulas take different forms for the two cases at hand. In what follows, we present the method of our calculation in some detail.

A. One particle per unit cell

In this case, the possible candidate structures are represented by a two-dimensional unit cell that is repeated periodically over the space. In full generality, the unit cell is a parallelogram formed by the vectors \mathbf{a} and \mathbf{b} that sustain an angle ψ between them, as shown in Fig. 3. The position of an arbitrary particle on the lattice site is given by the linear combination $\mathbf{r} = l\mathbf{a} + m\mathbf{b}$, where l and m are integers. Introducing a coordinate system (xy) and choosing the x axis parallel to the unit-cell vector \mathbf{a} , the components r_x and r_y of the vector $\mathbf{r} = (r_x, r_y)$ can be written as follows: $r_x = \alpha l + \beta m$, $r_y = \gamma m$, where we have introduced parameters $\alpha = a$, $\beta = b \cos \psi$ and $\gamma = b \sin \psi$, with ψ being the angle between the vector \mathbf{b} and the x axis. Having inserted the explicit expressions of particle positions in Eq. (3), the energy

U_1 in Eq. (6) takes the form of a lattice sum $\sum_{l=-\infty}^{\infty} \sum_{m=-\infty}^{\infty} (\dots)$ running over integers l and m , with the combination $(l,m)=(0,0)$ being excluded. In order to find stable structures of solid that correspond to the lowest total energy, we need to minimize the lattice sum with respect to all free variational parameters. In the case at hand, there are α , β , and γ , which are introduced above for convenience instead of unit-cell parameters a , b , and ψ . Working at a fixed density n acts as a constraint that eliminates one of those due to the relationship $\alpha=1/\gamma n$, therefore we are left with the two parameters β and γ . One additional variational parameter δ is the angle between the in-plane magnetic field

component \mathbf{B}_{\parallel} and the x axis (see Fig. 3), which characterizes the relative orientation of the magnetic dipoles with respect to a lattice direction in the crystal.

While the short-ranged Lennard-Jones term $\sum u^{\text{LJ}}(r)$ does not cause any problems during computation, the long-ranged dipole-dipole interaction summation $\sum u^{\text{dip}}(\mathbf{r}, \mathbf{B}_0)$ converges slowly and it takes too long time to obtain the required accuracy of the resulting value. To accelerate convergence, we rewrite the series $\sum u^{\text{dip}}(\mathbf{r}, \mathbf{B}_0)$ in terms of the modified Bessel functions $K_0(x)$ and $K_1(x)$ following the Lekner method. Making use of the substitutions proposed by Lekner [24], it is straightforward to derive the expression

$$\begin{aligned} \frac{2}{(\chi B_0)^2} \sum_{\mathbf{r} \neq 0} u^{\text{dip}}(\mathbf{r}, \mathbf{B}_0) &= \sum_{\substack{l,m=-\infty \\ (l,m) \neq (0,0)}}^{\infty} \frac{1}{[(\alpha l + \beta m)^2 + (\gamma m)^2]^{3/2}} \left[1 - 3 \cos^2 \varphi \frac{[(\alpha l + \beta m) \cos \delta + (\gamma m) \sin \delta]^2}{(\alpha l + \beta m)^2 + (\gamma m)^2} \right] \\ &= [1 - \cos^2 \varphi (1 + \sin^2 \delta)] \frac{16\pi}{\alpha^2 \gamma} \sum_{l=1}^{\infty} \sum_{m=1}^{\infty} \frac{l}{m} \cos\left(2\pi \frac{\beta}{\alpha} lm\right) K_1\left(2\pi \frac{\gamma}{\alpha} lm\right) \\ &\quad + \cos^2 \varphi \cos(2\delta) \frac{32\pi^2}{\alpha^3} \sum_{l=1}^{\infty} \sum_{m=1}^{\infty} l^2 \cos\left(2\pi \frac{\beta}{\alpha} lm\right) K_0\left(2\pi \frac{\gamma}{\alpha} lm\right) \\ &\quad - \cos^2 \varphi \sin(2\delta) \frac{32\pi^2}{\alpha^3} \sum_{l=1}^{\infty} \sum_{m=1}^{\infty} l^2 \sin\left(2\pi \frac{\beta}{\alpha} lm\right) K_1\left(2\pi \frac{\gamma}{\alpha} lm\right) + [1 - \cos^2 \varphi (1 + \sin^2 \delta)] \frac{2}{3} \frac{\pi^2}{\alpha \gamma^2} \\ &\quad + (1 - 3 \cos^2 \varphi \cos^2 \delta) \frac{2}{\alpha^3} \zeta(3), \end{aligned} \tag{7}$$

where $\zeta(x)$ is the Riemann zeta function. The use of the right-hand side of Eq. (7) instead of the original expression drastically improves the convergence speed and allows for a very fast computation of the energy U_1 during its minimization procedure. The lattice structures minimizing the energy U_1 with respect to variational parameters β , γ , δ span in this way the five two-dimensional Bravais lattices, namely the triangular, square, rectangular, rhombic [25], and oblique lattices. The results of the minimization procedure are presented in the following section.

B. Two particles per unit cell

The second possible class of candidate structures we consider are generated by the periodic repetition of a unit cell, defined as above by \mathbf{a} , \mathbf{b} , and ψ , having one more additional particle placed inside the parallelogram. The position of the added particle is specified by the vector $\mathbf{c}=(c_x, c_y)$. When such a cell is repeated periodically over the space, it produces two lattices shifted with respect to each other by the vector \mathbf{c} , as shown in Fig. 3. In other words, we are dealing here with lattices possessing a two-particle basis. The positions of the particles of the first lattice on the (x,y) plane are given by the vectors $\mathbf{r}=(\alpha l + \beta m, \gamma m)$, while the sites of the

second lattice are located at the points $\mathbf{r}+\mathbf{c}=(\alpha l + \beta m + c_x, \gamma m + c_y)$, where l, m are integers and $\alpha=a$, $\beta=b \cos \psi$, $\gamma=b \sin \psi$. The class of such structures includes, among others, the honeycomb and ‘‘herringbone’’ structures as possible lattices, as well as periodic repetitions of two-chain bundles, similar to those observed in Monte Carlo simulations in the fluid phase [18].

For this system the total energy per particle reads as

$$U_2 = U_1 + \frac{1}{2} \sum_{\mathbf{r} \neq 0} [u^{\text{dip}}(\mathbf{r} + \mathbf{c}, \mathbf{B}_0) + u^{\text{LJ}}(|\mathbf{r} + \mathbf{c}|)], \tag{8}$$

which is the energy U_1 , given by Eq. (6), of a particle interacting with all other particles within its own sublattice, plus the additional energy of interaction with the other sublattice. Once more, the set $\{\mathbf{r}\}$ spans a Bravais lattice. The parameters characterizing the lattice structure are α , β , γ , c_x , and c_y . The constraint of constant particle density allows to eliminate the parameter $\alpha=2/\gamma n$. As before, we do not fix the direction of the magnetic field with respect to the lattice axis and allow for the variation of δ , the angle between \mathbf{B}_{\parallel}

and the x axis. The stable crystal structures are found by minimization of energy U_2 with respect to the parameters β , γ , δ , c_x , and c_y .

To achieve rapid convergence of the dipolar series in Eq.

(8), we apply the Lekner method [24] as in the preceding section. Accordingly, the slowly converging sum $\sum u^{\text{dip}}(\mathbf{r} + \mathbf{c}, \mathbf{B}_0)$ is written in terms of the modified Bessel functions $K_0(x)$ and $K_1(x)$ as follows:

$$\begin{aligned}
& \frac{2}{(\chi B_0)^2} \sum_{\mathbf{r} \neq 0} u^{\text{dip}}(\mathbf{r} + \mathbf{c}, \mathbf{B}_0) \\
&= \sum_{l, m = -\infty}^{\infty} \frac{1}{[(\alpha l + \beta m + c_x)^2 + (\gamma m + c_y)^2]^{3/2}} \left[1 - 3 \cos^2 \varphi \frac{[(\alpha l + \beta m + c_x) \cos \delta + (\gamma m + c_y) \sin \delta]^2}{(\alpha l + \beta m + c_x)^2 + (\gamma m + c_y)^2} \right] \\
&= [1 - \cos^2 \varphi (1 + \sin^2 \delta)] \frac{8\pi}{\alpha^2} \sum_{l=1}^{\infty} \sum_{m=-\infty}^{\infty} \frac{l}{|\gamma m + c_y|} \cos\left(\frac{2\pi l}{\alpha}(\beta m + c_x)\right) K_1\left(\frac{2\pi l}{\alpha}|\gamma m + c_y|\right) \\
&\quad + \cos^2 \varphi \cos(2\delta) \frac{16\pi^2}{\alpha^3} \sum_{l=1}^{\infty} \sum_{m=-\infty}^{\infty} l^2 \cos\left(\frac{2\pi l}{\alpha}(\beta m + c_x)\right) K_0\left(\frac{2\pi l}{\alpha}|\gamma m + c_y|\right) \\
&\quad - \cos^2 \varphi \sin(2\delta) \frac{16\pi^2}{\alpha^3} \sum_{l=1}^{\infty} \sum_{m=-\infty}^{\infty} l^2 \frac{(\gamma m + c_y)}{|\gamma m + c_y|} \sin\left(\frac{2\pi l}{\alpha}(\beta m + c_x)\right) K_1\left(\frac{2\pi l}{\alpha}|\gamma m + c_y|\right) \\
&\quad + [1 - \cos^2 \varphi (1 + \sin^2 \delta)] \frac{2\pi^2}{\alpha \gamma^2 \sin^2(\pi c_y / \gamma)}, \tag{9}
\end{aligned}$$

where $(\alpha l + \beta m + c_x, \gamma m + c_y) \neq (0, 0)$.

For $\gamma m + c_y > 0$ the first three summations of the right-hand side of Eq. (9) can be obtained directly from Eq. (7) by making use of the substitutions $\beta m \rightarrow \beta m + c_x$ and $\gamma m \rightarrow \gamma m + c_y$, which correspond to a shift in the coordinate space: $r_x \rightarrow r_x + c_x$, $r_y \rightarrow r_y + c_y$. However, the last terms of Eqs. (7) and (9), corresponding to $r_x = 0$ or $r_y = 0$, are totally different.

During the calculation of the lattice sum, it can happen that the argument of the Bessel functions becomes small. In this case, the values of the Bessel functions are large and too many terms of the series will be necessary to add in order to obtain the required precision. We cope with this problem following the approach proposed in Ref. [26], namely we rewrite both summations (7) and (9) in a different coordinate system $(x'y')$. While in the coordinate system (xy) the direction of the vector \mathbf{a} coincides with the x axis, in the new coordinates $(x'y')$ the y' axis is directed along the vector \mathbf{b} , see Fig. 3. The transformation between the two coordinate systems is the rotation around z axis by the angle $\pi/2 - \psi$. It is easy to derive the substitutions that are necessary for rewriting the right-hand sides of Eqs. (7) and (9) in the new coordinate system: $\alpha \rightarrow \alpha' = \sqrt{\beta^2 + \gamma^2}$, $\beta \rightarrow \beta' = \alpha\beta / \sqrt{\beta^2 + \gamma^2}$, $\gamma \rightarrow \gamma' = \alpha\gamma / \sqrt{\beta^2 + \gamma^2}$, $\sin \delta \rightarrow \sin(\psi - \delta)$, $\cos \delta \rightarrow \cos(\psi - \delta)$, $c_x \rightarrow c'_x = c_x \cos \psi + c_y \sin \psi$, and $c_y \rightarrow c'_y = c_x \sin \psi - c_y \cos \psi$. After making these substitutions, the expression of summations will change and the arguments of Bessel functions will take different values, leaving, however,

the value of the lattice sum (total energy of the system) invariant with respect to the rotation of the coordinate system. Thus, switching between the two representations of summations allows us to achieve fast convergence. In general, there are infinitely many coordinate systems that can be chosen for the representations of the series (7) and (9).

To find the energy minimum we used the Powell method, the initial input for which was the approximate minimum found by scanning through the grid in the space of minimization parameters. Finally, we remark that the minimization with respect to the lattice vectors does not automatically produce the shortest ones, so that the resulting crystal structure is not always automatically recognizable. In order to remedy this shortcoming, we calculate subsequently the *shortest* linearly independent vectors \mathbf{a}_{\min} and \mathbf{b}_{\min} that span the given lattice. Their lengths are given as $a_{\min} = \min_k |\mathbf{b} - k\mathbf{a}|$ and $b_{\min} = \min_l |\mathbf{a}_{\min} - l\mathbf{b}|$, where k and l are integers. In what follows, we adopt the convention $a_{\min} \geq b_{\min}$.

IV. RESULTS AND DISCUSSION

We have carried out the minimizations of U_1 and U_2 [Eqs. (6) and (8)] with respect to the corresponding variational parameters and found the stable crystal structures for various values of parameters λ , n^* , and φ . Our numerical calculation has shown that both sums U_1 and U_2 have exactly the same minima with the same crystal phases over the whole parameter space. In other words, the optimal value of

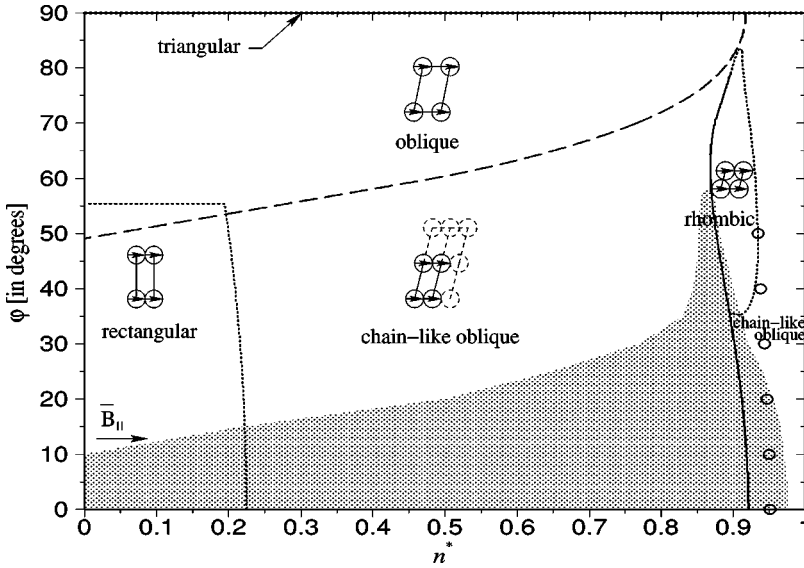


FIG. 4. The phase diagram in the (n^*, φ) plane at magnetic field strength $\lambda = 3$. The dotted (solid) lines denote continuous (discontinuous) transitions. The dashed line, termed “unsticking line” in the text, indicates second-order transition from the oblique phase to the chainlike oblique; for a quantitative characterization of these phases, see the text. The open circles denote a continuous transition within the chainlike oblique phase. The gray region denotes phase separation between the phases lying at the two opposite boundaries for a given value of φ . Accordingly, the transitions denoted by the lines that penetrate this region are preempted by it but they are nevertheless shown in order to demonstrate the development of the structural changes of the lattice at all φ values.

the variational quantity \mathbf{c} that describes the positioning of the basis is always such that a Bravais lattice is generated and there are no stable periodic non-Bravais arrangements with a nontrivial two-particle basis for the system at hand. Though this does not rule out the existence of structures with a larger number of basis members, it acts as an indication that the system prefers the simpler periodic Bravais structures. A wealth of those appears in the phase diagram nevertheless.

First, we note that for all stable lattice structures that minimize the energy, the direction of the in-plane component of the magnetic field, \mathbf{B}_{\parallel} , coincides with that of the shortest elementary lattice vector. This result is in agreement with results obtained by Monte Carlo [18] and molecular dynamics [27] simulations.

We begin with the phase diagram for a value of the coupling parameter $\lambda = 3$, presented in Fig. 4. In the absence of anisotropic interactions, $\varphi = 90^\circ$, the radially symmetric repulsion gives rise to a triangular lattice, as expected by the fact that the latter possesses optimal packing properties. Upon deviation of the magnetic field angle from the value $\varphi = 90^\circ$, the anisotropy of the interaction induces a continuous transformation of the triangular lattice into an oblique one with two unequal lattice constants, and with the in-plane component of the dipoles, \mathbf{m}_{\parallel} , oriented along the shorter lattice vector. At low values of the angle φ , the strongly attractive dipolar interactions cause a broad coexistence region that terminates at a critical point for a tilt angle $\varphi \cong 60^\circ$.

The broad phase coexistence region can be suppressed by reducing the value of λ , as will be discussed later. In order to obtain some insight into the mechanisms bringing about the stability of the various phases, we neglect for now this coexistence region and focus our attention on the structural characteristics of the oblique phase at arbitrary values of n^* and φ . There exist further phase transitions within this phase and, in order to characterize them, we introduce the ratio a_{\min}/b_{\min} between the two lattice constants as a suitable order parameter.

As can be seen in Fig. 5, upon increasing the angle φ

from 0° to 90° , the size ratio a_{\min}/b_{\min} shows cusps at different values of φ , depending on the density n^* . At the low- φ part the size ratios are large and decrease monotonically upon increasing φ . In fact, for low- φ values, the parameter b_{\min} remains practically constant for all densities at a value that almost coincides with the minimum of the total interaction potential for a head-to-tail orientation of the dipoles, see Fig. 6. The particles form, therefore, *chains* with a constant bead-to-bead distance, whereas an increase of the density simply reduces the value of a_{\min} , bringing those chains closer together. In view of this fact, we characterize the oblique lattice in the region below the line delineated by the locus of cusps in the parameter a_{\min}/b_{\min} as *chainlike oblique*. Above the aforementioned line, the particles forming the chains “unstuck.” The physical reason for this lies in the increasingly strong repulsions that take place as φ grows and which do not favor such a high degree of anisotropy any-

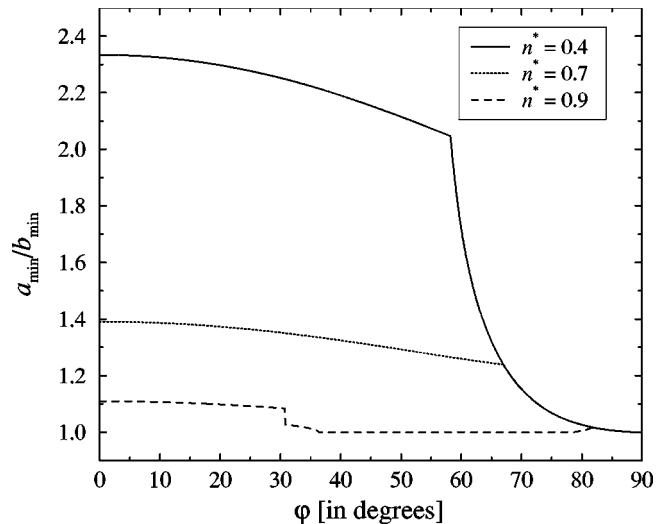


FIG. 5. The aspect ratio a_{\min}/b_{\min} between the shortest unit vectors vs the tilt angle φ , for various values of dimensionless density n^* and for $\lambda = 3$.

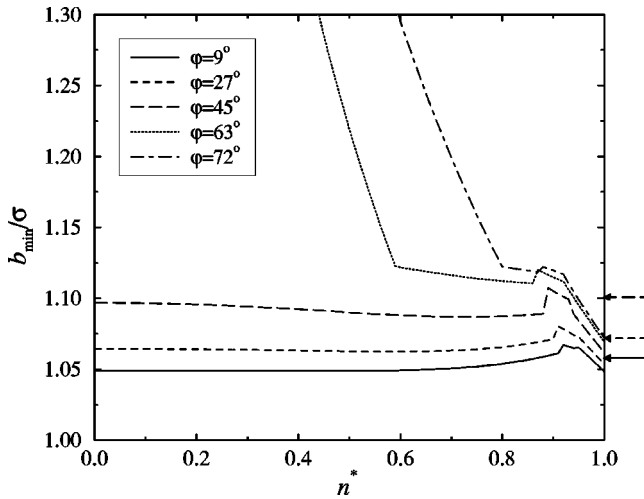


FIG. 6. Dependence of the shortest lattice constant b_{\min} on the density at $\lambda=3$. The arrows on the right denote the position r_{\min} of the total interaction potential $u^{\text{dip}} + u^{\text{LJ}}$ for a head-to-tail configuration. The arrow lines are coded in the same way as the curves on the plot, corresponding thereby to the values of φ indicated in the legend. For the angles $\varphi=63^\circ$ and 72° , such a minimum does not exist.

more as the one present in the chain phase. As can be seen in Fig. 7, in the oblique phase the size ratio remains at a constant (but φ -dependent) value for all values of the density, thus a change of n^* there simply causes the oblique unit cell to shrink uniformly. The reason for this behavior lies therein, that in this part of the phase diagram the short-range steric repulsion $u^{\text{LJ}}(r)$ is not felt by the particles, which interact instead exclusively by means of the dipolar interaction $u^{\text{dip}}(\mathbf{r}, \mathbf{B}_0)$, Eq. (3). Since the latter has the form of a scale-free power law, the average density sets the only length scale

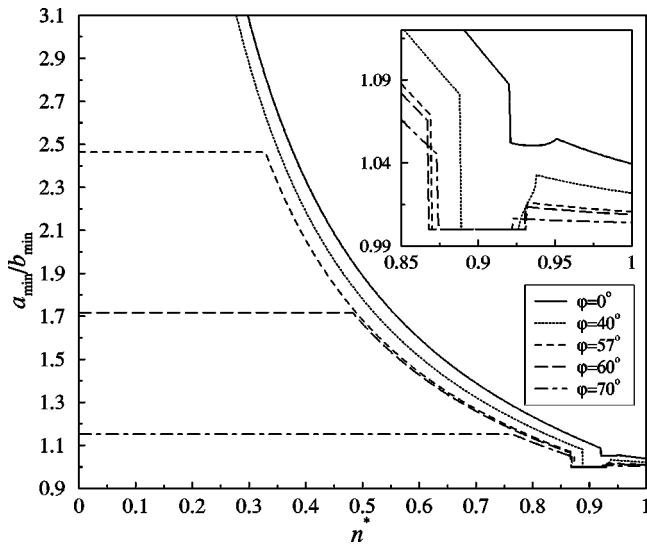


FIG. 7. The aspect ratio a_{\min}/b_{\min} between the shortest unit vectors vs dimensionless density n^* for various values of the tilt angle φ and for $\lambda=3$. The inset shows the high-density part of the diagram in more detail and its axes carry the same labels as those of the main plot.

and the effect of changing n^* is merely a shrinking of the lattice. In the chainlike oblique phase, on the other hand, the smaller lattice constant b_{\min} is essentially density independent and only a_{\min} changes. We locate, therefore, a line of “unsticking transitions” through the phase diagram that splits the oblique phase into two domains, the regular oblique and the chainlike oblique. We will discuss the physical origin of this line shortly.

The same line goes also through a region of the phase diagram in which the rectangular lattice is stable and which occurs typically for $n^* \leq 0.25$ and $\varphi < 56^\circ$. Upon increase of n^* , the rectangular lattice transforms continuously into the chainlike oblique one, since a staggered configuration of the long chains becomes then energetically more favorable than the parallel one [18]. At the high-density part of the phase diagram and for angles $35^\circ \leq \varphi \leq 78^\circ$, a first-order transition from the chainlike oblique to the rhombic lattice takes place, as can be seen from the inset of Fig. 7: the aspect ratio a_{\min}/b_{\min} displays there a jump to the value unity. At lower φ values, the first-order transition line continues, separating now two chainlike oblique phases from one another. We emphasize here that at densities $n^* \geq 0.9$, the particles are densely packed and thus there are no chains to be recognized anymore. Nevertheless, we still characterize the high-density phase of the system as chainlike oblique because there is a path in the phase diagram that goes around the rhombic phase, still lying below the unsticking line, which connects the high-density region with the low-density chainlike oblique phase without crossing any phase boundaries. This path cannot be clearly discerned in Fig. 4 because it is very narrow due to the close proximity of the unsticking line with the upper tip of the rhombic phase area; but it exists nevertheless. Within the high-density chainlike oblique phase, another, continuous phase transition takes place, as witnessed by a further cusp in the aspect ratio that can be seen in the inset of Fig. 7. This transition is denoted by the open circles in Fig. 4.

We have also calculated the phase diagrams for other values of the coupling parameter λ ; representative results are shown in Figs. 8 and 9. The topology of the phase diagram remains the same. One important quantitative difference occurs for the coexistence region at the bottom of the phase diagram. This becomes broader for $\lambda=10$ but disappears altogether for $\lambda=0.0001$ since in the latter case the dipole-dipole attractions are very weak.

The location of the “unsticking line” remains exactly the same in the range $\lambda=0.0001, \dots, 1000$. This demonstrates that the physical origin of this line lies exclusively in the dipolar interaction and has nothing to do with the presence of the Lennard-Jones cores. Indeed, within the whole range of stability of the oblique phase, the particle positions are such that the nearest neighbors of the lattice find themselves at distances larger than the cutoff distance $2^{1/6}\sigma$ of the Lennard-Jones potential. The colloids interact, therefore, exclusively by means of the dipolar interaction which causes the transition to the chainlike oblique phase along the unsticking line. Only inside the chainlike oblique phase do nearest neighbors approach close enough so that the steric repulsion is felt and then the competition between the anisotropic and the radially

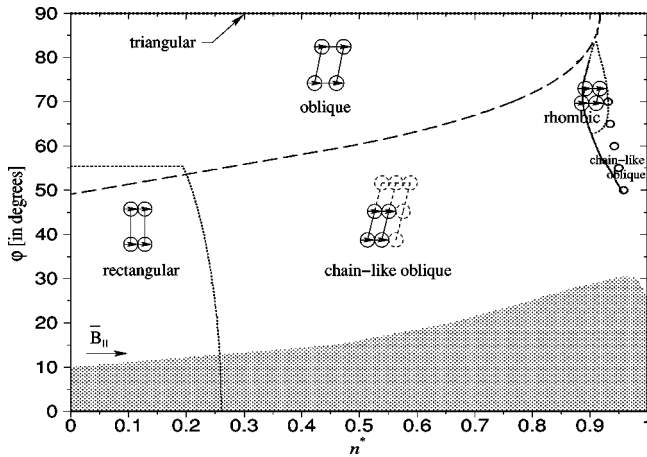


FIG. 8. The phase diagram in the (n^*, φ) plane for magnetic field strength $\lambda = 10$. The meaning of the various lines is the same as in Fig. 4.

symmetric interactions gives rise to alterations of the phase boundaries. In particular, as can be seen from Figs. 8 and 9, an increase in λ causes the region of stability of the rhombic phase to shrink, since it increases the strength of the orientationally dependent potential that favors lattices with unequal lattice constants. Moreover, an increase in λ causes a slight expansion of the domain of stability of the rectangular phase towards higher densities.

V. CONCLUSIONS

In conclusion, we have calculated the phase diagram of a two-dimensional suspension of superparamagnetic colloids in a tilted external magnetic field in the limit where thermal fluctuations are small. Depending on the tilt angle and the particle concentration, we find a wealth of different stable two-dimensional crystal lattices including rectangular, oblique, chainlike oblique, and rhombic structures. These predicted structures should be verified in experimental investigations and could be interesting to fabricate nanosieves

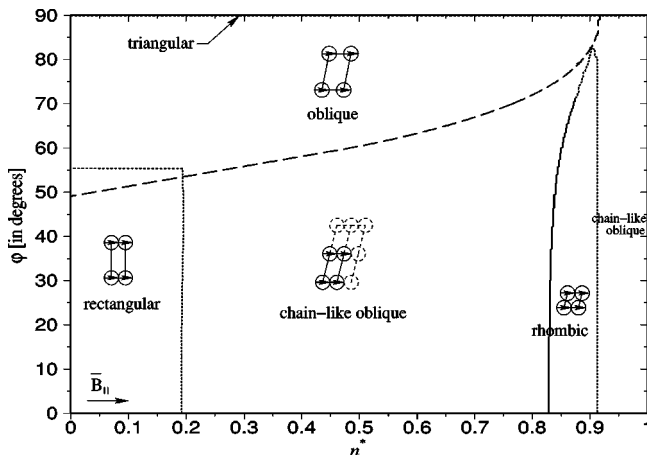


FIG. 9. The phase diagram in the (n^*, φ) plane at magnetic field strength $\lambda = 0.001$. The meaning of the various lines is the same as in Fig. 4.

[28,29], photonic crystals, and microfluidic devices.

Further future investigations should focus on the following open problems: first, the elastic constants of the crystal can be calculated within lattice sums. In particular, it would be interesting to examine the anisotropy of the elastic behavior for anisotropic crystalline structures. Second, one should consider the effect of a finite temperature. It would be very interesting, in particular, to check how the KTNHY scenario is affected in melting anisotropic two-dimensional crystal lattices. Furthermore, the question whether there is a stable chain liquid at finite temperature should be thoroughly explored. Finally, the present methods can be transferred to *three-dimensional* oriented or unoriented dipolar systems. This would be of great interest for ferrofluids [30]. Indeed, various crystalline structures have recently been obtained in theory [31–34] and experiments [35–38] but a full comprehensive understanding including a possible fluid phase of chains is not available at the moment. This is a challenge for the future.

ACKNOWLEDGMENTS

This work was supported by the Deutsche Forschungsgemeinschaft (DFG), within subproject C3 of the SFB-TR6 program, “Physics of colloidal dispersions in external fields.” We thank S. Dietrich, J. J. Weis, S. Odenbach, and R. Messina for helpful discussions.

APPENDIX: THE HAMILTONIAN OF TWO MAGNETIC (ELECTRIC) DIPOLES IN A SPATIALLY INHOMOGENEOUS EXTERNAL FIELD

In this appendix we derive the formula of potential energy of two polarizable permeable (dielectric) objects placed in external magnetic (electric) fields.

As a first step, let us consider the situation in which an object of finite volume V_1 and magnetic permeability μ_1 is introduced into a magnetic field $\mathbf{B}_0(\mathbf{r})$ in a linear medium of magnetic permeability μ_0 . We assume that the object is neutral and there are no external current densities. Affected by the field, the object becomes polarized, forming a magnetic dipole and changing the field from $\mathbf{B}_0(\mathbf{r})$ to $\mathbf{B}'(\mathbf{r})$ in all space. The total energy of such a system is [39]

$$u' = \frac{1}{8\pi} \int \mathbf{B}' \cdot \mathbf{H}' d^3r, \quad (\text{A1})$$

where the integration is performed over the whole space. The quantity u' can be rewritten as

$$u' = I'_1 + I'_2 + u^{\mathbf{B}_0},$$

where we have introduced the notations I'_1 , I'_2 , and $u^{\mathbf{B}_0}$ as

$$I'_1 = \frac{1}{8\pi} \int (\mathbf{B}' - \mathbf{B}_0) \cdot (\mathbf{H}' + \mathbf{H}_0) d^3r,$$

$$I'_2 = \frac{1}{8\pi} \int (\mathbf{B}_0 \cdot \mathbf{H}' - \mathbf{B}' \cdot \mathbf{H}_0) d^3r,$$

$$u^{\mathbf{B}_0} = \frac{1}{8\pi} \int \mathbf{B}_0 \cdot \mathbf{H}_0 d^3r. \quad (\text{A2})$$

The integral I'_1 vanishes by the following argument. Since there are no free currents (apart from the fixed currents producing the initial field \mathbf{B}_0), we have from the magnetostatics Maxwell equations that $\nabla \times \mathbf{H}' = 0$. Therefore, a magnetic scalar potential Φ_M can be introduced, $\mathbf{H}' = -\nabla \Phi_M$. Expressing the integrand of I'_1 through $\nabla \Phi_M$ and performing integration by parts, one obtains that $I'_1 = 0$.

Let us now calculate I'_2 by splitting the integration space into V_1 and the outer volume of V_1 . Since the medium is linear in its magnetic properties, we have the following relations: inside the volume V_1 , $\mathbf{H}_0 = \mathbf{B}_0/\mu_0$, $\mathbf{H}' = \mathbf{B}'/\mu_1$ and outside the volume V_1 , $\mathbf{H}_0 = \mathbf{B}_0/\mu_0$, $\mathbf{H}' = \mathbf{B}'/\mu_0$. As a result, the nonvanishing part of the integral I'_2 remains only over the volume V_1 :

$$I'_2 = -\frac{1}{2} \int_{V_1} \frac{1}{4\pi} \left(\frac{1}{\mu_0} - \frac{1}{\mu_1} \right) \mathbf{B}' \cdot \mathbf{B}_0 d^3r = u^{\mathbf{d}_1 \mathbf{B}_0}.$$

We introduce new notation $u^{\mathbf{d}_1 \mathbf{B}_0}$ in order to make clear the physical meaning of the integral I'_2 . In free space, $\mu_0 = 1$. Making use of the definition of the magnetization [39], $\mathbf{M}_1 = (1/4\pi)(1 - 1/\mu_1)\mathbf{B}'$, we rewrite $u^{\mathbf{d}_1 \mathbf{B}_0}$ as

$$u^{\mathbf{d}_1 \mathbf{B}_0} = -\frac{1}{2} \int_{V_1} \mathbf{M}_1 \cdot \mathbf{B}_0 d^3r. \quad (\text{A3})$$

Thus, the energy of the system ‘‘external field + polarizable object’’ reads as

$$u' = u^{\mathbf{d}_1 \mathbf{B}_0} + u^{\mathbf{B}_0},$$

where $u^{\mathbf{d}_1 \mathbf{B}_0}$ [Eq. (A3)] is the energy of interaction between the magnetic dipole $\mathbf{M}_1(\mathbf{r})$ and the field $\mathbf{B}_0(\mathbf{r})$, and $u^{\mathbf{B}_0}$ [Eq. (A2)] is the initial magnetostatic energy.

At the second step of our derivation, we place an object of volume V_2 and magnetic permeability μ_2 into the magnetic field $\mathbf{B}'(\mathbf{r})$, which is the field (considered above) in the presence of one permeable object. Introducing a second object will change the field from $\mathbf{B}'(\mathbf{r})$ to $\mathbf{B}(\mathbf{r})$. The energy of such a system is

$$u = \frac{1}{8\pi} \int \mathbf{B} \cdot \mathbf{H} d^3r.$$

We express u through I_1 , I_2 , and u' as

$$u = I_1 + I_2 + u',$$

where

$$I_1 = \frac{1}{8\pi} \int (\mathbf{B} - \mathbf{B}') \cdot (\mathbf{H} + \mathbf{H}') d^3r,$$

$$I_2 = \frac{1}{8\pi} \int (\mathbf{B}' \cdot \mathbf{H} - \mathbf{B} \cdot \mathbf{H}') d^3r,$$

and u' is given by Eq. (A1).

The integral I_1 vanishes by the same argument as I'_1 . The integral I_2 is zero within the volume V_1 and in the space outside V_1 and V_2 , since $\mathbf{H}' = \mathbf{B}'/\mu_i$, $\mathbf{H} = \mathbf{B}/\mu_i$, where $i = 0, 1$. I_2 remains nonzero only within the volume V_2 where $\mathbf{H}' = \mathbf{B}'/\mu_0$ and $\mathbf{H} = \mathbf{B}/\mu_2$. Therefore we have

$$I_2 = -\frac{1}{2} \int_{V_2} \frac{1}{4\pi} \left(\frac{1}{\mu_0} - \frac{1}{\mu_2} \right) \mathbf{B} \cdot \mathbf{B}' d^3r.$$

The magnetization $\mathbf{M}_2(\mathbf{r})$ of the second object is defined as $\mathbf{M}_2 = (1/4\pi)(1 - 1/\mu_2)\mathbf{B}$. The field outside the volume V_1 is $\mathbf{B}' = \mathbf{B}_0 + \mathbf{B}_{d_1}$, with the magnetic dipole field

$$\mathbf{B}_{d_1}(\mathbf{r}') = \int_{V_1} \frac{3[\mathbf{M}_1(\mathbf{r}) \cdot \mathbf{n}]\mathbf{n} - \mathbf{M}_1(\mathbf{r})}{|\mathbf{r} - \mathbf{r}'|^3} d^3r,$$

obtained as the dipolar contribution in the multipole expansion [39], which can be applied for large separations as compared to the linear size of the object. Here $\mathbf{n} = (\mathbf{r} - \mathbf{r}')/|\mathbf{r} - \mathbf{r}'|$. Thus we have

$$I_2 = u^{\text{dd}} + u^{\mathbf{d}_2 \mathbf{B}_0},$$

where $u^{\mathbf{d}_2 \mathbf{B}_0}$ is the dipole-field interaction energy,

$$u^{\mathbf{d}_2 \mathbf{B}_0} = -\frac{1}{2} \int_{V_2} \mathbf{M}_2 \cdot \mathbf{B}_0 d^3r \quad (\text{A4})$$

and u^{dd} is the dipole-dipole interaction energy:

$$u^{\text{dd}} = \frac{1}{2} \int_{V_1} d^3r \int_{V_2} d^3r' \times \frac{\mathbf{M}_1(\mathbf{r}) \cdot \mathbf{M}_2(\mathbf{r}') - 3[\mathbf{M}_1(\mathbf{r}) \cdot \mathbf{n}][\mathbf{M}_2(\mathbf{r}') \cdot \mathbf{n}]}{|\mathbf{r} - \mathbf{r}'|^3}. \quad (\text{A5})$$

Collecting all necessary terms, we finally obtain the energy u of two polarizable objects of finite arbitrary geometries in external spatially inhomogeneous magnetic fields as

$$u = u^{\text{dd}} + u^{\mathbf{d}_1 \mathbf{B}_0} + u^{\mathbf{d}_2 \mathbf{B}_0} + u^{\mathbf{B}_0}, \quad (\text{A6})$$

where the dipole-dipole interaction energy u^{dd} , the dipole-field interaction energies $u^{\mathbf{d}_i \mathbf{B}_0}$ ($i = 1, 2$) and initial field energy $u^{\mathbf{B}_0}$ are specified by Eqs. (A5), (A3), (A4), and (A2).

Note that the factor 1/2 in Eqs. (A3)–(A5) is traced to the linear relation between \mathbf{M} and \mathbf{B} and acquires its physical explanation from the fact that the dipoles are not permanent but rather induced by the external field.

For the case of pointlike dipoles and making use of the magnetic moment definition

$$\mathbf{m}_i = \int_{V_i} \mathbf{M}_i(\mathbf{r}) d^3r,$$

Eq. (A5) reduces to Eq. (1).

The expression for the energy of two polarizable dielectrics in external electric field can be readily derived making use of the electrostatic Maxwell equations and following the

same approach as for magnetostatics above. The result one obtains are Eqs. (A2)–(A6), where the place of the magnetic fields \mathbf{B} , \mathbf{H} , and magnetization \mathbf{M} will be taken by the electric fields \mathbf{E} , \mathbf{D} , and polarization \mathbf{P} , respectively.

-
- [1] P. Pieranski, Phys. Rev. Lett. **45**, 569 (1980).
- [2] D.Y.C. Chan, J.D. Henry, and L.R. White, J. Colloid Interface Sci. **79**, 410 (1981).
- [3] N.D. Denkov, O.D. Velev, P.A. Kralchevsky, I.B. Ivanov, H. Yoshimura, and K. Nagayama, Nature (London) **361**, 26 (1993).
- [4] H.H. Wickman and J.N. Korley, Nature (London) **393**, 445 (1998).
- [5] P.A. Kralchevsky and N.D. Denkov, Curr. Opin. Colloid Interface Sci. **6**, 383 (2001).
- [6] M.G. Nikolaidis, A.R. Bausch, M.F. Hsu, A.D. Dinsmore, M.P. Brenner, C. Gay, and D.A. Weitz, Nature (London) **420**, 299 (2002).
- [7] Y. Lin, H. Skaff, T. Emrick, A.D. Dinsmore, and T.P. Russell, Science **299**, 226 (2003).
- [8] K. Zahn and G. Maret, Curr. Opin. Colloid Interface Sci. **4**, 60 (1999).
- [9] H. Löwen, J. Phys.: Condens. Matter **13**, R415 (2001).
- [10] K. Zahn, J.M. Méndez-Alcaraz, and G. Maret, Phys. Rev. Lett. **79**, 175 (1997).
- [11] H. Löwen, Phys. Rep. **237**, 249 (1994).
- [12] K. Strandburg, Rev. Mod. Phys. **60**, 161 (1988).
- [13] K. Zahn, R. Lenke, and G. Maret, Phys. Rev. Lett. **82**, 2721 (1999).
- [14] K. Zahn and G. Maret, Phys. Rev. Lett. **85**, 3656 (2000).
- [15] K. Zahn, A. Wille, G. Maret, S. Sengupta, and P. Nielaba, Phys. Rev. Lett. **90**, 155506 (2003).
- [16] A. Wille, F. Valmont, K. Zahn, and G. Maret, Europhys. Lett. **57**, 219 (2002).
- [17] G. Maret (private communication).
- [18] A. Satoh, R.W. Chantrell, S.-I. Kamiyama, and G.N. Coverdale, J. Colloid Interface Sci. **178**, 620 (1996).
- [19] K. Wojciechowski and J. Klos, J. Phys. A **29**, 3963 (1996).
- [20] F. Rothen and P. Pieranski, Phys. Rev. E **53**, 2828 (1996).
- [21] G.T. Gao, X.C. Zeng, and W. Wang, J. Chem. Phys. **106**, 3311 (1997).
- [22] S.H.L. Klapp and M. Schoen, J. Chem. Phys. **117**, 8050 (2002).
- [23] J.J. Weis, J.M. Tavares, and M.M. Telo da Gama, J. Phys.: Condens. Matter **14**, 9171 (2002).
- [24] J. Lekner, Physica A **157**, 826 (1989).
- [25] In standard terminology, one speaks of the *centered rectangular* lattice which is, however, identical to a rhombic one. e.g., see J.S. Blakemore, *Solid State Physics*, 2nd ed. (Cambridge University Press, Cambridge, 1985).
- [26] A. Grzybowski and A. Brodka, Mol. Phys. **100**, 1017 (2002).
- [27] H. Löwen *et al.*, in *Proceedings of the Third International Symposium on Slow Dynamics in Complex Systems*, edited by M. Tokuyama and I. Oppenheim (AIP, New York, 2003).
- [28] W.A. Goedel, Europhys. Lett. **62**, 607 (2003).
- [29] W.A. Goedel and H. Xu, Langmuir **19**, 4950 (2003).
- [30] *Ferrofluids, Magnetically Controllable Fluids and Their Applications*, edited by S. Odenbach, Lecture Notes in Physics Vol. 594 (Springer, Berlin, 2002).
- [31] L. Zou, W. Wen, and P. Sheng, Phys. Rev. Lett. **81**, 1509 (1998).
- [32] S. Klapp and F. Forstmann, Phys. Rev. E **60**, 3183 (1999).
- [33] B. Groh and S. Dietrich, Phys. Rev. E **63**, 021203 (2001).
- [34] Z. Wang, C. Holm, and H.W. Müller, Phys. Rev. E **66**, 021405 (2002).
- [35] W. Wen, N. Wang, H. Ma, Z. Lin, W.Y. Tam, C.T. Chan, and P. Sheng, Phys. Rev. Lett. **82**, 4248 (1999).
- [36] U. Dassanayake, S. Fraden, and A. van Blaaderen, J. Chem. Phys. **112**, 3851 (2000).
- [37] A. Yethiraj and A. van Blaaderen, Nature (London) **421**, 513 (2003).
- [38] K. Butter, P.H.H. Bomans, P.M. Frederik, G.J. Vroege, and A.P. Philipse, Nat. Mater. **2**, 88 (2003).
- [39] J.D. Jackson, *Classical Electrodynamics* (Wiley, New York, 1975).